UC Irvine
UC Irvine Previously Published Works

Title
RECENT DEVELOPMENTS IN FREQUENCY-DOMAIN FLUOROMETRY

Permalink
https://escholarship.org/uc/item/3mf7n519

Journal
ANALYTICAL INSTRUMENTATION, 14(3-4)

ISSN
0743-5797

Authors
LAKOWICZ, JR
MALIWAL, BP
GRATTON, E

Publication Date
1985

Copyright Information

Peer reviewed

RECENT DEVELOPMENTS IN FREQUENCY-DOMAIN FLUOROMETRY

Joseph R. Lakowicz and Badri P. Maliwal

University of Maryland
School of Medicine
Department of Biological Chemistry
Baltimore, Maryland 21201

and

Enrico Gratton

University of Illinois
Department of Physics
Urbana, Illinois 61801

I. SUMMARY

Phase-modulation fluorometry is the frequency-domain analogue of time-resolved fluorescence spectroscopy. During the past three years we witnessed the development of variable-frequency phase-modulation fluorometers with modulation frequencies from 1 to 220 MHz. These instruments provide impressive resolution of multi or non-exponential fluorescence decays. To introduce these instruments we describe their design and operational principles. To illustrate the obtainable resolution we present results for the resolution of two and three-component mixtures of fluorophores, the resolution of complex anisotropy decays from non-spherical

molecules and the determination of time-resolved emission spectra in the presence of time-dependent spectral relaxation. At present, the resolution obtainable with the frequency-domain fluorometers appears to be at least equivalent to that obtained with pulsed mode-locked laser sources with single photon counting. These mode-locked sources can also be used for phase fluorometry, as described elsewhere in this volume by Gratton and co-workers.

II. INTRODUCTION

Fluorescence spectroscopy is often used in biochemical research because of its high inherent sensitivity and the suitable time scale of the phenomenon [1,2]. Fluorescence emission typically occurs within nanoseconds of light absorption, which is also the timescale of many dynamic processes in biochemical samples. These processes include decay of the fluorescence intensity, rotational diffusion of proteins and membrane-bound fluorophores and spectral relaxation of biopolymer-bound fluorophores. Because of the complexity of biological macromolecules or heterogeneous samples it is often necessary to resolve multi-exponential decays of fluorescence intensity or anisotropy. For example, the decay times of fluorophores are sensitive to their local environment. Also, biological macromolecules often contain fluorophores in several distinct locations. It is desirable to resolve the emitting species, which is accomplished by resolution of the decay law of the fluorescence emission. Similarly, the rotational diffusion of macromolecule-bound fluorophores depends upon the size, shape and rigidity of the rotating unit. These dynamic properties of the macromolecule can be revealed by the time-resolved decays of fluorescence anisotropy.

In principle, resolution of the time-dependent decays of intensity or anisotropy can be accomplished using either time domain or frequency domain measurements. In the time-domain one

measures the time-dependent response of the sample following pulsed excitation. In the frequency-domain one measures the phase angle and modulation of the emission relative to the intensity modulated incident light. During the past 15 years there has been considerable progress and emphasis on time-domain measurements. This is because of the sensitivity and accuracy of time-correlated single-photon counting [3,4], continued advances in time resolution and precision resulting from the use of mode-locked and cavity-dumped laser light sources [5-9], and because of the use of microchannel plate photomultiplier tubes with subnanosecond response times. Recent instruments are now capable of resolving closely spaced fluorescence lifetimes [6,7].

At present, phase-modulation fluorometry is less widely utilized for the resolution of complex fluorescence decays. This is somewhat surprising in that phase-modulation fluorometers were constructed prior to the development of time-domain instruments [10-14]. It is rather easy to measure small phase shifts with good precision. Hence, phase fluorometers are especially useful for measurement of subnanosecond lifetimes. However, until recently, these instruments operated at only one to three fixed frequencies. Even with very precise data, the limited number of frequencies did not allow the resolution of complex decays of intensity or anisotropy [15]. We note that some successful resolutions have been accomplished [16-18]. In this respect, phase sensitive detection has been found particularly useful [17,19], and recently it has become possible to resolve three lifetime components using phase sensitive spectra at a single modulation frequency [20]. However, the resolution of multiple lifetimes using phase sensitive spectra relies upon knowing, at least approximately, the steady state spectra of the individual components. Because of these limitations phase-modulation fluorometers have not provided, in a general way, for the resolution of complex decay laws.

Recently, several laboratories described phase-modulation fluorometers capable of operation at continuously variable

frequencies [21-25]. The designs described by Gratton [21] and
Lakowicz [22] which use a laser source and a electrooptic
modulator provide good precision in the phase and modulation data,
and hence good resolution of the fluorescence decays. For
instance, instruments based on this design have been used to
resolve two and three decay times from mixtures of fluorophores
[22,26], to resolve three component decays of anisotropy [27], to
measure rotational correlation times as short as 47 psec [22], and
to construct time-resolved emission spectra of membrane and
protein-bound fluorophores [28-29].

In the following sections we summarize the operational
features of our frequency-domain fluorometer. Such instruments
can be easily constructed using commercially available
components. Only a minor amount of specialized circuitry is
required. Additionally, we present data which illustrates the
methods of data analysis and the resolving power of the frequency-
domain method. Our approach to analysis is based on nonlinear
least squares [30-31]. Fitting is performed directly in the
frequency domain [32].

A FREQUENCY-DOMAIN FLUOROMETER

Since the technique of frequency-domain is relatively new, we
briefly describe our instruments. Additional details may be found
elsewhere [21-22]. A schematic description of the instrument is
shown in Figure 1. The output of a CW-laser is intensity
modulated in an approximate sinusoidal manner at a frequency F.
The intensity modulated light excites the sample, and the emission
is observed using a photomultiplier. Another PMT is placed near a
quartz beam splitter and is used as a phase reference. This PMT
can also be positioned in the T-format location for differential
polarized phase measurements. Measurement of the phase angle
differnce between the sample and reference emission is
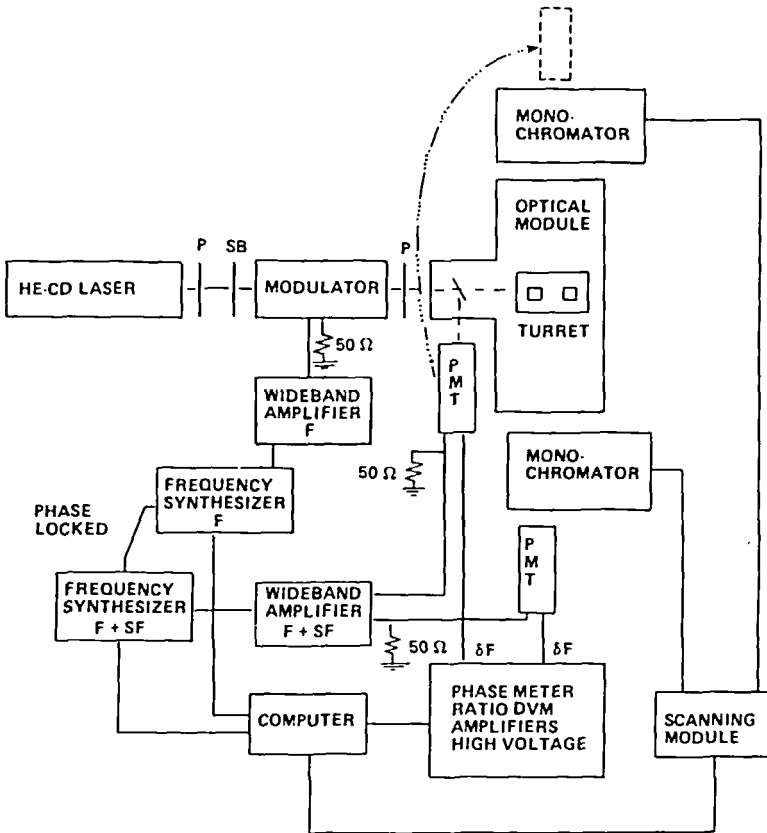accomplished by rotation of a turret. The phase angle difference

Figure 1.

Schematic of the Variable-Frequency Phase-Modulation Fluorometer.

P, polarizer; B, Soleil-Babinet compensator; F, frequency; δF, cross-correlation frequency; PMT, photomultiplier tube. From [22].

(ϕ_ω) and the relative modulation of the sample (m_ω) can be measured relative to either scattered light or a reference fluorophore [33]. The subscript ω refers to the modulation frequency, expressed in radians per second ($\omega = 2\pi F$). Detection of the emission is performed using the cross correlation principle [14]. Generation of the cross-correlation frequency is accomplished differently than originally described by Spencer and Weber (14) and provides su perior resolution [21,22]. Specifically, the gain of the PMTs is modulated at the frequency F + 25 Hz, where F is the modulation frequency of the incident light. The phase and modulation are measured at the 25 Hz cross correlation frequency by a time-interval counter and a ratio digital volt meter, respectively. The two closely spaced frequencies are provided by two frequency synthesizers which are each driven by the same crystal reference source (phase locked). The data are averaged and stored by an interfaced Apple IIe computer. Measurement at 20 modulation frequencies typically requires 1 hour.

Intensity modulation of the laser light is accomplished using an electro-optic modulator. In response to an applied electric field these devices change linearly polarized light into circularly polarized light. The theory and operation of these devices has been described previously [34-35]. The electro-optic modulator is placed between crossed polarizers (Figure 2). We use a Soleil-Babinet compensator (SB) to provide an optical bias. An advantage of the SB compensator compared to a fixed retardation plate is that any degree of bias can be obtained at any wavelength. This is functionally equivalent to the voltage bias shown in Figure 3.

The functional properties of the modulator and its associated optics are shown in Figure 3. If an RF voltage is applied to the modulator, and no optical or electrical bias is applied, then the transmitted light is modulated at twice the applied frequency (Figure 3 top). We have not used this doubling procedure because
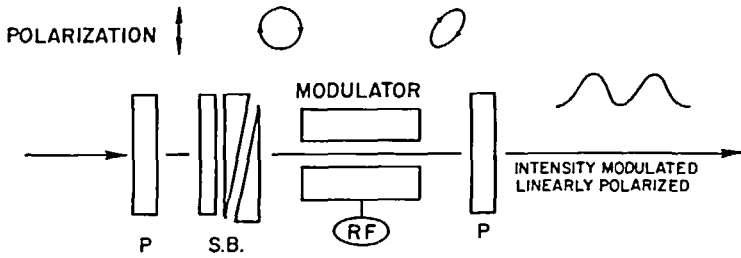
POLARIZATION

Figure 2.

Optical Arrangement for an Electro-Optic Modulator.

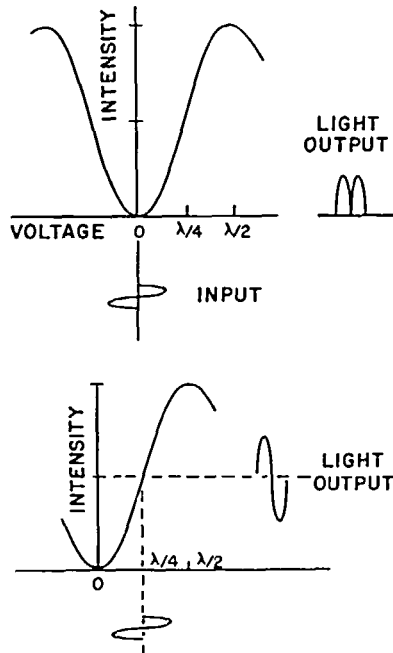P, polarizer; SB, Soleil-Babinet Compensator; RF, radio frequency signal. From [22].

Figure 3

Modulated Intensity from an Electro-Optic Modulator.

The upper drawing shows the modulated intensity without an .electrical or optial bias, the lower drawing includes a λ/4 bias. From [22].

we consistently obtained higher modulation with a comparable
frequency range with the non-doubling mode. We use the modulators
in the approximate linear mode (Figure 3 bottom). This can be
accomplished using either a voltage bias or an optical bias. The
linearly polarized light is transformed into elliptically
polarized light by the SB compensator (Figure 2). If the SB
compensator is adjusted to the $\lambda/4$ position then the light
incident on the modulator is circularly polarized. When a voltage
is applied the polarization is rotated further. Hence, the
transmission is varied, and the incident light is modulated at the
applied frequency (Figure 3).

ANALYSIS OF FREQUENCY-DOMAIN DATA

A. Resolution of Multi-Exponential Decays of Intensity

We presently use the method of nonlinear least squares for
estimation of the decay times from the frequency-domain data. For
a mixture of n fluorophores, each of which displays a single
lifetime, the impulse function $(I(t))$ is a sum of exponential
decays

$$I(t) = \sum_i^n \alpha_i e^{-t/\tau_i}. \tag{1}$$

In this expression τ_i is the decay of the i'th component and α_i is
the preexponential factor of this component. The fractional
contribution of each component to the steady state intensity is
given by

$$f_i = \frac{\alpha_i \tau_i}{\sum_i \alpha_i \tau_i} \tag{2}$$

At each modulation frequency the expected values of the phase
angle $\phi_{c\omega}$ and the modulation $m_{c\omega}$ are given by [36,37]

$$\phi_{C\omega} = \text{arc tan } (N_\omega / D_\omega) \tag{3}$$

$$m_{C\omega} = (N_\omega^2 + D_\omega^2)^{1/2} \tag{4}$$

where $\omega = 2\pi \times$ frequency (in cycles per second), and

$$N_\omega J = \sum_i^n \frac{\alpha_i \, \omega \, \tau_i^2}{1 + \omega^2 \, \tau_i^2} \tag{5}$$

$$D_\omega J = \sum_i^n \frac{\alpha_i \, \tau_i}{1 + \omega^2 \, \tau_i^2} \tag{6}$$

and

$$J = \sum_i \alpha_i \, \tau_i. \tag{7}$$

The goodness of fit between the measured values and an assumed model is judged by the value of χ^2, which is given by

$$\chi^2 = \sum_\omega \frac{1}{\sigma_{\phi\omega}^2} (\phi_\omega - \phi_{C\omega})^2 + \sum_\omega \frac{1}{\sigma_{m\omega}^2} (m_\omega - m_{C\omega})^2 \tag{8}$$

In this expression $\sigma_{\phi\omega}$ and $\sigma_{m\omega}$ are the errors of the measured phase and modulation values under the chosen experimental conditions.

A more familiar measure of the goodness-of-fit is the value of reduced χ^2,

$$\chi_R^2 = \frac{\chi^2}{\nu} = \frac{\chi^2}{2N - p} \tag{9}$$

where the number of degrees of freedom is given by $\nu = 2N - p$. N is the number of modulation frequencies and p is the number of

floating parameters. If the assumed model is appropriate for the
sample, and if the errors are random and properly estimated by $\sigma_{\phi\omega}$
and $\sigma_{m\omega}$, then χ^2_R is expected to be near unity.

B. Decays of Fluorescence Anisotropy

Time-resolved anisotropies can be determined from the phase
difference (Δ_ω) between the perpendicular ($\phi_\perp$) and parallel ($\phi_{\parallel}$)
components of the modulated emission ($\Delta_\omega = \phi_\perp - \phi_{\parallel}$) and the
amplitude ratio (Λ_ω) of the parallel ($m_{\parallel}$) and the perpendicular
($m_\perp$) components of the modulated emission ($\Lambda = m_{\parallel}/m_\perp$). The
decays of the parallel ($\parallel$) and perpendicular ($\perp$) components of
the emission are given by

$$I_{\parallel}\ (t) = \frac{1}{3}\ I\ (t)\ (1 + 2r\ (t))\tag{10}$$

$$I_{\perp}\ (t) = \frac{1}{3}\ I\ (t)\ (1 - 2r\ (t))\tag{11}$$

where $r(t)$ is the time-resolved decay of anisotropy. Generally,
$r(t)$ can be described as a multi-exponential decay,

$$r(t) = r_0 \sum_i g_i\ e^{-t/\theta_i}\tag{12}$$

where r_0 is the limiting anisotropy in the absence of rotational
diffusion and θ_i are the rotational correlation times. The
expected values of Δ_ω ($\Delta_{c\omega}$) and Λ_ω ($\Lambda_{c\omega}$) can be calculated from
the sine and cosine transforms of the individual polarized decays
[2,36,37].

$$N_i = \int_0^\infty I_i\ (t)\ \sin \omega t\ dt\tag{13}$$

$$D_i = \int_0^\infty I_i\ (t)\ \cos \omega t\ dt\tag{14}$$

Where i can be the parallel or perpendicular component of the decay. The frequency-dependent values of Δ_ω and Λ_ω are given by

$$\Delta_{c\omega} = \arctan \left(\frac{D_{||} N_\perp - N_{||} D_\perp}{N_{||} N_\perp + D_{||} D_\perp}\right) \tag{15}$$

$$\Lambda_{c\omega} = \left(\frac{N_{||}^2 + D_{||}^2}{N_\perp^2 + D_\perp^2}\right)^{1/2} \tag{16}$$

where the N_i and D_i are calculated at each frequency. The parameters describing the anisotropy decay are obtained by minimizing the squared deviations between measured and calculated values,

$$\chi^2 = \sum_\omega \frac{1}{\sigma_{\Delta\omega}^2} \left(\Delta_\omega - \Delta_{c\omega}\right)^2 + \sum_\omega \frac{1}{\sigma_{\Lambda\omega}^2} \left(\Lambda_\omega - \Lambda_{c\omega}\right)^2 \tag{17}$$

In this expression $\sigma_{\Delta\omega}$ and $\sigma_{\Lambda\omega}$ are the estimated experimental uncertainties in the measured quantities (Δ_ω and Λ_ω).

We used two models to describe the decays of anisotropy. For an isotropic rotator we used

$$r(t) = r_0 e^{-t/\theta}. \tag{18}$$

For the anisotropic rotator perylene we used an anisotropy decay law with two or three correlation times,

$$r(t) = r_0 \sum_i g_i e^{-t/\theta_i}. \tag{19}$$

with $\sum_i g_i = 1$, g_i as floating parameters and r_0 fixed. In some cases the floating parameters were $r_0 g_i$. More details are given in [27].

C. Time-Resolved Emission Spectra

Construction of time-resolved emission spectra from the frequency-domain data is a straightforward extension of the analysis of multi-exponential decays. The time-resolved emission spectra can be calculated from the impulse response functions, if these are known at each emission wavelength. In our case the impulse response functions were determined using measurements of the phase ($\phi_\omega(\lambda)$) and modulation ($m_\omega(\lambda)$) of the emission, over a range of emission wavelengths (λ) and modulation frequencies (ω). Typically, we used about 10 emission wavelengths and 10 modulation frequencies for each wavelength. These data were fit, using the method of non-linear least squares to the function

$$I(\lambda,t) = \sum_{i=i}^{3} \alpha_i(\lambda)\, e^{-t/\tau_i(\lambda)} \qquad (20)$$

The decay at each emission wavelengths λ is probably more complex than a sum of exponentials. However, we found that a three-exponential decay was quite adequate to represent the measured quantities, and hence adequate for the construction of the time-resolved spectra.

Calculation of the time-resolved emission spectra requires that the impulse response functions be normalized [38,2]. Specifically, the total intensity at each wavelength must be normalized to the steady state intensity at this same wavelength ($F(\lambda)$). Let

$$H(\lambda) = \frac{F(\lambda)}{\int_0^\infty I(\lambda,t)\, dt} \qquad (21)$$

$$= \frac{F(\lambda)}{\alpha_1(\lambda)\,\tau_1 + \alpha_2(\lambda)\,\tau_1 + \alpha_3(\lambda)\,\tau_3} \qquad (22)$$

Then, the appropriately normalized functions are given by

$$I'(\lambda,t) = H(\lambda) \ I(\lambda,t) \tag{23}$$

$$= \sum_i \alpha_i'(\lambda) \ e^{-t/\tau_i} \tag{24}$$

where $\alpha_i'(\lambda) = H(\lambda) \ \alpha_i(\lambda)$. For any desired time (t_i), the time-resolved emission spectrum is obtained by plotting the values of $I'(\lambda,t_i)$ for all the measured wavelengths. In these spectra we normalized the peak intensities to allow easy visualization of the time-dependent spectral shifts.

III. RESULTS AND DISCUSSION

A. Single Exponential Decays of Intensity

The data in Figure 4 illustrates the use of frequency-domain data for measurement of single exponential decay times. The data are for fluorescein in water (4.3 nsec) and for rose bengal in ethanol (0.83 nsec) and in water (0.13 nsec). At any given frequency larger phase angles and smaller modulations are seen for the longer lifetimes. The phase angles increase and the modulation decreases with increasing modulation frequency. The solid lines (top panel) represent the theoretical curves calculated for the lifetimes which yielded minimum value of x_R^2. Obviously, the calculated values for single exponential decay accurately reproduce the measured values ($\bullet$, o, $\blacktriangle$). The agreement between the measured and calculated data is further illustrated in the lower panel of Figure 4, which shows the deviations between the measured data and the calculated values. The deviations are randomly distributed around zero. This indicates that the single exponential model is adequate to account for the data, and that the measurements are free of systematic errors. The average deviations are near 0.2 degrees for phase and 0.002 for
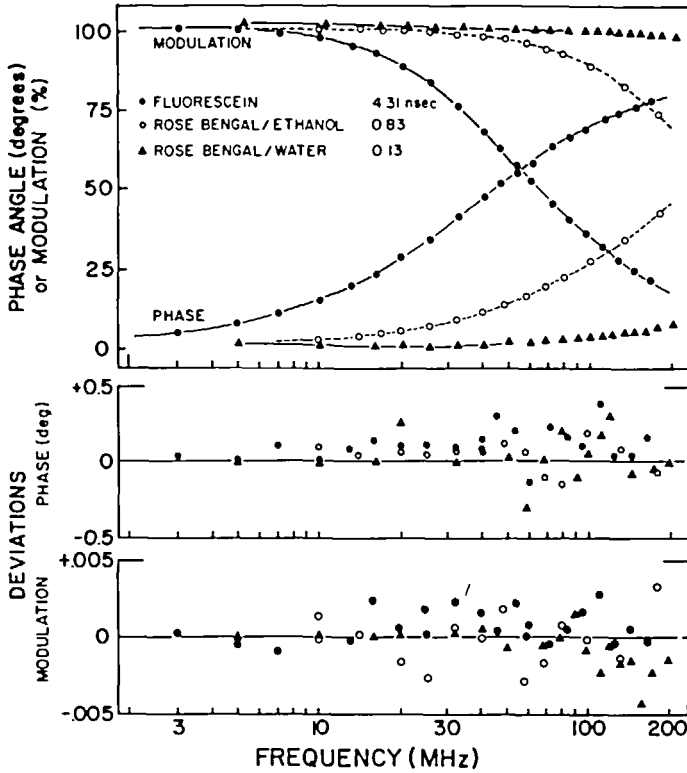
Figure 4

Phase and Modulation Data for Single-Component Solutions.

Data are shown for fluorescein in water (0.02M tris, pH = 8) (●), rose bengal in ethanol (o) and in water (▲). The lower panel shows the deviations between the measured and calculated values. From [22].

modulation, using the instrument described in [22]. Somewhat
higher random deviations were found using the earlier measurements
(21,26), probably due to our limited experience with the
instruments. We found these random errors, or smaller, to be the
apparent level of random error for most of our measurements.
These values were used for the calculation of x_R^2. In contrast to
photon counting data [3,39], the random errors in phase and
modulation are not be estimated on the basis of counting
statistics. Rather, we estimate the level of random error by
comparison of the data with the calculated values for cases in
which the assumed decay law is appropriate. The fact that x_R^2 are
often less than unity indicates that the actual level of random
error is less than 0.2 degrees of phase and less than 0.002 in
modulation.

We attempted to fit the data for fluorescein and rose bengal
to double exponential decays of intensity. The values of x_R^2 did
not substantially decrease, and the amplitude of the assumed
second component was negligible. Such results demonstrate that
inclusion of an additional component is not justified from the
data. These results illustrate the precision and accuracy of our
measurements. They do not appear to be any significant systematic
errors which result in the apparent detection of small additional
components in the decay law. We note that these measurements were
performed without use of standard fluorophores [33], indicating
the absence of significant color or geometric artifacts in the
time response of the photomultiplier tubes (21,22).

B. <u>Resolution of Multi-Exponential Decays</u>

In our opinion the major challenge is not measurement of the
shortest lifetimes. In biochemical research it is more important
to resolve closely spaced decay times. Since the decay times (τ_i)
and preexponential factors (α_i) are correlated parameters, one
requires precise measurements to obtain reliable estimates of α_i

and τ_i. To illustrate the resolution obtainable from the frequency-domain measurements we examimned several two-component mixtures [22,26]. One such resolution is shown in Figure 5 for a mixture of POPOP (1.32 nsec) and 9-cyanoanthracene, (9-CYANT, 12.12 nsec). Obviously, a good fit to the measured data (•) is provided by an assumed two-component decay law (————), whereas the single component decay law is completely inadequate to account for the data (---).

The lower panels show the deviations between the measured and calculated values for the best fit obtainable using a single (--•--) and double (-o-) exponential decay law. For this mixture, in which the decay times differ by 10-fold, the experimental deviations found using a single decay time are about 20 to 100-fold larger than the random error level of the measurements. For the single-component fit the deviations vary systematically with the frequency, indicating that the deviations are not due to random error and are probably due to an inappropriate decay law [32]. Additionally, the value of x_R^2 = 421 is clearly unacceptable. The inclusion of a second component in the decay law results in a 600-fold decrease in x_R^2 to 0.80, and the deviations become small and randomly distributed around zero. Importantly, the calculated decay times and fractional intensities (1.36 and 12.05 nsec, 0.47 and 0.53) are in good agreement with the expected values (1.32 and 12.12 nsec, $f_1 = f_2 = 0.5$).

We note that lifetimes more closely spaced than 1.3 and 12.1 nsec can also be resolved. For instance, we resolved two lifetimes which differed by only 50% (4.1 and 6.3 nsec) with a 50-fold decrease in x_R^2 [22]. Furthermore, using a method analogous to the Global method of Brand and co-workers [40], we resolved a two component decay with lifetimes differing by only 8%, 4.1 and 4.4 nsec [22]. To the best of our knowledge these are the most closely spaced lifetimes which have been resolved to date, excluding those resolved by phase sensitive detection in which the emission spectra of the components were known.
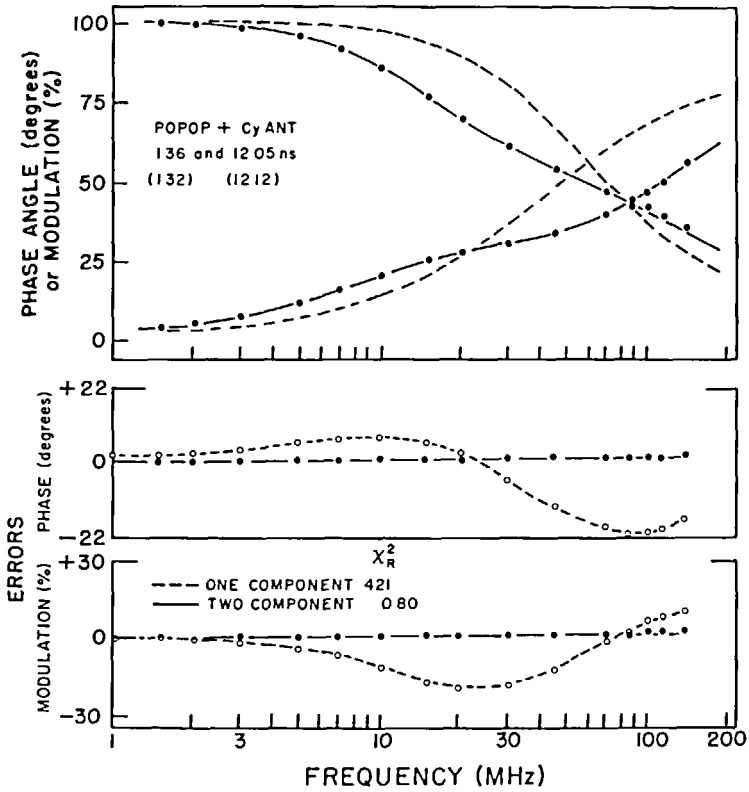
Figure 5

Phase and Modulation Data for a Mixture of POPOP and 9-Cyanoanthracene

The dashed line indicate the best one-component fit, and the solid line the best two-component fit. The values not in parenthesis are the experimental values and those in parenthesis are from measurements on the pure components. From [26].

It is well known that the resolution of a three-component decay is considerably more difficult than a two-component decay [41]. Hence, it was of interest to test our instrument using a three-component mixture. We examined three-component mixtures of POPOP (1.32 nsec), methylanthracene (4.44 nsec) and 9-cyanoanthracene (12.12 nsec). The resolution of a 3-component mixture with a 10-fold range of lifetimes is a difficult problem. Figure 6 shows the two and three-component fits to the three-component mixture. The two-component fit is easily judged to be unsuccessful because of the systematically varying deviations and the large value of x_R^2. The two-component fit displays deviations which are about 5-fold larger than the expected level of random error. Inclusion of the third component yields a 21-fold decrease in x_R^2 and more random deviations.

C. Determination of Subnanosecond Anisotropy Decays

Frequency-domain fluorometry is uniquely suited for the measurement of anisotropy decays. This is because it allows for direct measurement of the phase angle different between the parallel ($\parallel$) and the perpendicular ($\perp$) components of the emission. This feature can be compared with time-correlated photon counting, in which it is necesarry to calculate the intensity difference between the polarized components following the individual measurements. The advantage of direct determination of the difference signal is evident from the measurements of subnanosecond anisotropy decays.

To illustrate this ability of frequency-domain fluorometry we examined POPOP in low viscosity solvents. The phase angle different (Δ_ω) between the perpendicular ($\phi_\perp$) and parallel ($\phi_\parallel$) components of the emisison ($\Delta_\omega = \phi_\perp - \phi_\parallel$) are shown in Figure 7. The differential polarized phase angle (Δ_ω) is dependent upon the rotational rate. For a single correlation time a plot of Δ_ω versus log ω is nearly Lorentzian in shape. This is not evident in Figure 7 because the rotational rate of POPOP is fast in these solvents, and the maximum value of Δ_ω is displaced beyond our
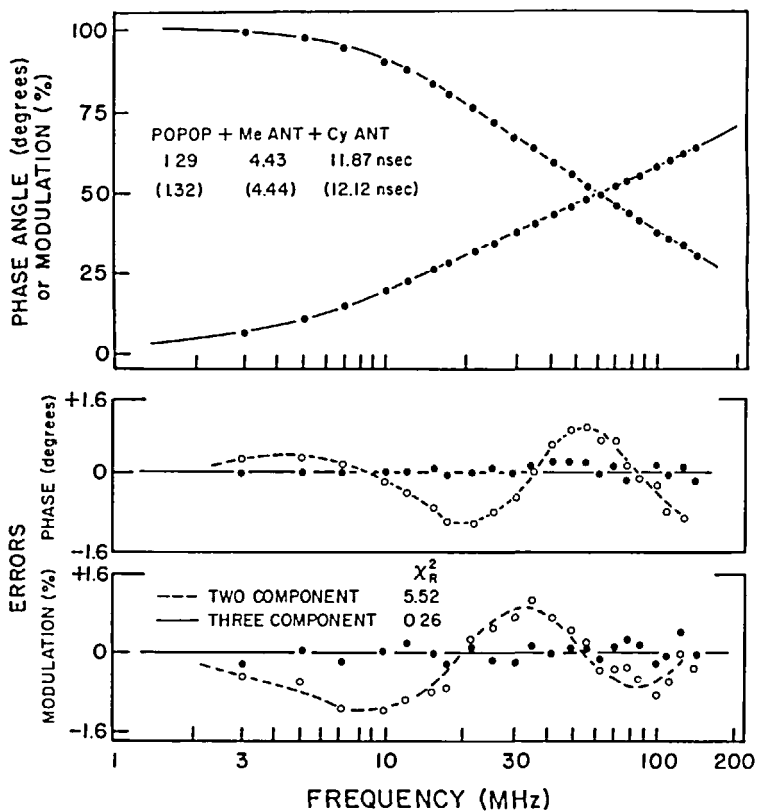
Figure 6

Phase and Modulation Data for a Three-Component Mixture of POPOP, 9-Methylanthracene and 9-cyanoanthracene.

The fractional intensities of the three components are equal $(f_1 = f_2 = f_2 = 0.33)$.   See Figure 5 for details.   From [26].

maximum frequency of 200 MHz. The solid lines represent the calculated values of Δ_ω for the correlation times shown on Figure 7. We could easily determine correlation times as short as 0.11 and 0.047 nsec for POPOP in ethanol and hexane at 45°C, respectively. To the best of our knowledge this is the shortest correlation time which has been directly measured, including measurements performed with mode-locked laser sources. For such rapid diffusive motions it is difficult to know if the decay of anisotropy is single or double exponential. In our measurements there was no substantial improvement in x_R^2 upon inclusion of an additional correlation time. It seems probable that the frequency range of our instrument can be extended to 400 MHz. Hence, the measurements may soon be directly comparable with molecular dynamics calculations on proteins.

D. Resolution of Multi-Exponential Decays of Fluorescence Anisotropy

There are many instances in which the anisotropy decay is expected to be more complex than a single exponential. Two important cases are due to the asymmetrical shapes of proteins and to the complex diffusive motions of probes in lipid bilayers. In these instances one attempts to recover the anisotropy decay parameters in order to characterize shape of the protein or the microenvironment in the membrane.

Preliminary data indicate that the frequency-domain fluorometry provides adequate resolution to determine the axial ratios of globular proteins. This is illustrated in Figure 8, which shows data for 9-aminoacridine in glycerol. Visually, the distinction between the one and two-correlation time fits to these data was modest. Statistically, the differences were substantial. At each temperature the value of x_R^2 decreased about 3-fold upon inclusion of the second correlation time. Additionally, at each temperature the ratio of the two correlation times was about 1.6. This result is significant in several ways. First, the
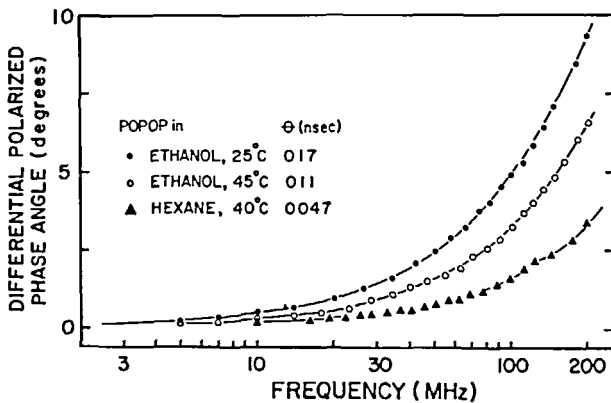
Figure 7

Differential Polarized Phase Angles for POPOP in Fluid Solvents.

Data are shown for POPOP in ethanol at 25 (•) and 41°C (o), and in hexane of °C (▲). From [22].

correlation times are in good agreement with those obtained by Barkley, Brand and co-workers [42]. However, these workers did not observe significant decreases in x_R^2, whereas our two correlation time fits are strongly supported by the analysis. We note that our results were significant without using Global analysis [40], whereas Brand and co-workers needed Global (multi-experiment) analysis to resolve the correlation times in a statistically significant manner. Secondly, many proteins have axial ratios in the range of 1.5 and above. Consequently, we expect the frequency-domain method to provide useful measurements of these axial ratios.

As our final example of a complex anisotropy decay we examined the anisotropic molecule perylene in DMPC bilayers [27]. Previous studies from this laboratory [43] indicated that below the transition temperature (<25°C) the rotational motions of perylene were hindered by the bilayer. Since perylene is itself
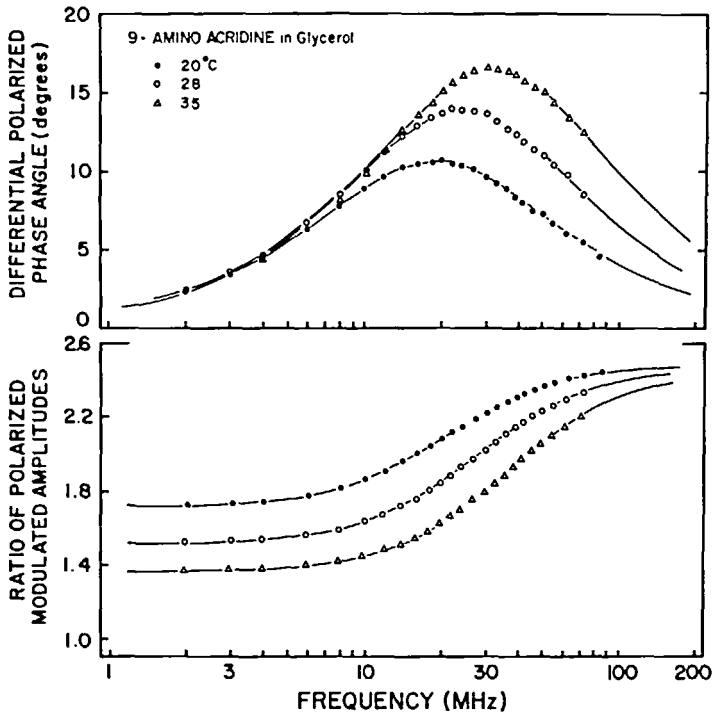
Figure 8

Differential Polarized Phase Angles and Modulation Ratios for 9-Aminoacridine in Glycerol.

At each temperature the ratio of the two correlation times is near 1.6, and χ_R^2 decreases about 3-fold for the two correlation time fit, relative to the one correlation time fit. From [22].

asymmetric, we predicted that three correlation times could be present. These data and fits are shown in Figure 9. The hindered model (---) was completely inadequate to account for the data (χ_R^2 = 106). Even the fit with two correlation times (———) is easily judged to be inadequate (χ_R^2 = 14.4). The three-correlation time fit provides a reasonable value of χ_R^2 = 0.5, and reasonable correlation times (0.2, 1.5 and 47 nsec). We attribute the two
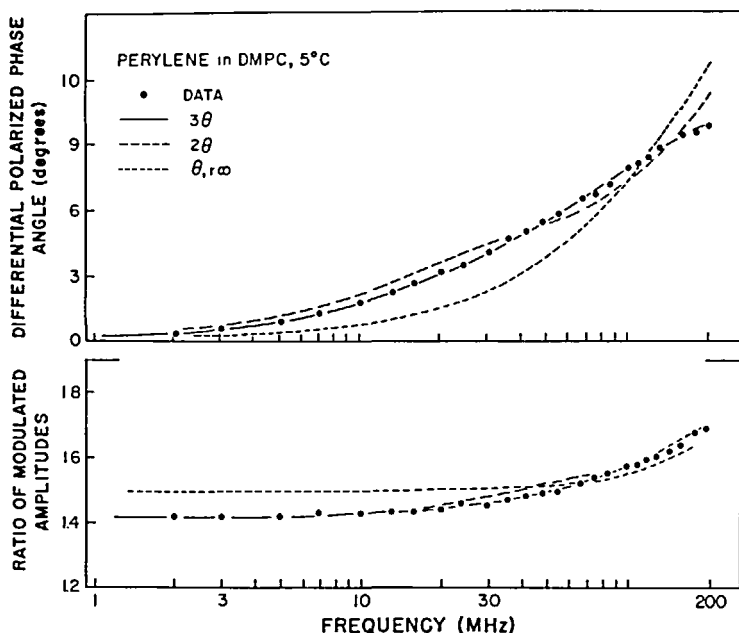
Figure 9.

Differential Polarized Phase Angles and Modulation Ratios for Perylene in DMPC Vesicles at 5°C.

The best fits are shown to the data (•) using the three correlation time model (———, $x_R^2 = 0.5$), the two-correlation time model (— —, $x_R^2 = 14.4$) and the hindered model (---, $x_R^2 = 106$). From [27].

shorter correlation times to rapid motions of perylene within the non-hindered environment, and the 47 nsec correlation time to the hindered motion. It is remarkable that one could obtain a 28-fold decrease in x_R^2 for distinguishing two versus three rotational correlation times. To the best of our knowledge this is the first published resolution of there rotational rates.

E. Time-Resolved Emission Spectra

Fluorophores in the excited state often undergo time-dependent interactions with their surroundings. For solvent-sensitive fluorophores such interactions result in time-dependent spectral shifts to lower energies or longer wavelengths [39,44-45]. A generally held view is that only pulse fluorescence methods are capable of yielding time-resolved emission spectra. We now know that frequency-domain fluorometry can reveal considerable detail about time-dependent spectral shifts [28-29]. To illustrate the capability of frequency-domain fluorometry for the determination of time-resolved emission spectra we present data for spectral relaxation of the probe TNS (2-p-toluidinyl-6-naphthalenesulfonic acid) in the viscous solvent glycerol and when bound in the heme site of apomyoglobin.

Frequency-dependent phase and modulation data for TNS dissolved in glycerol and bound to apomyoglobin are shown in Figure 10. These values are strongly dependent upon the emission wavelength. Larger phase angles and lower modulation are observed on the long wavelength side of the emission.

An important feature of these data is that the phase angles exceed 90°, which unambiguously demonstrate the presence of an excited state process which occurs subsequent to excitation [46]. This excited state process is the origin of the emission at longer wavelengths. We attribute the time-dependent spectral shift to reorientation of polar moieties of the solvent or protein in response to creation of the excited state of TNS.

Phase and modulation data were measured at 20-nm intervals from 400 to 540 nm. At each emission wavelength the data were analyzed in terms of a multi-exponential decay of fluorescence intensity. The solid lines in Figure 10 are calculated using three decay times. Clearly, the measured values can be closely approximated using this decay law. At the longest wavelengths (540 and 520 nm) the decay is almost a two-component decay with
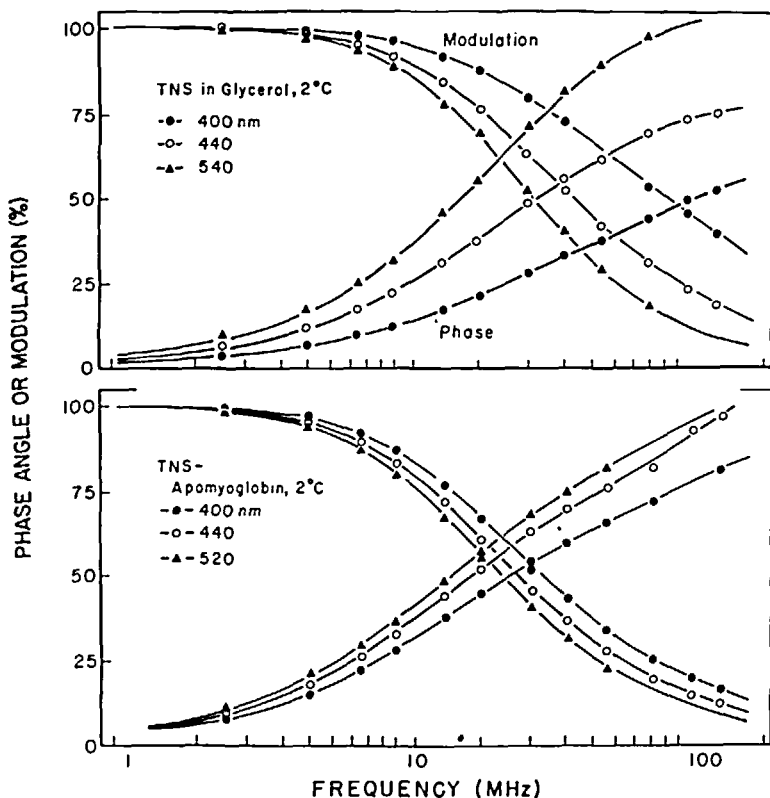
Figure 10

Frequency-Dependent Phase and Modulation Data for TNS in Glycerol
(top) and TNS-Bound to Apomyoglobin (bottom). From [27].

equal and opposite values of α_i [28]. These amplitudes indicate
that the observed fluorescence intensity is from the product of an
excited state process, with minimum contribution from the intially
excited state [47].

Time-resolved emission spectra can be calculated using the
steady-state emission spectra (not shown) and the impulse response
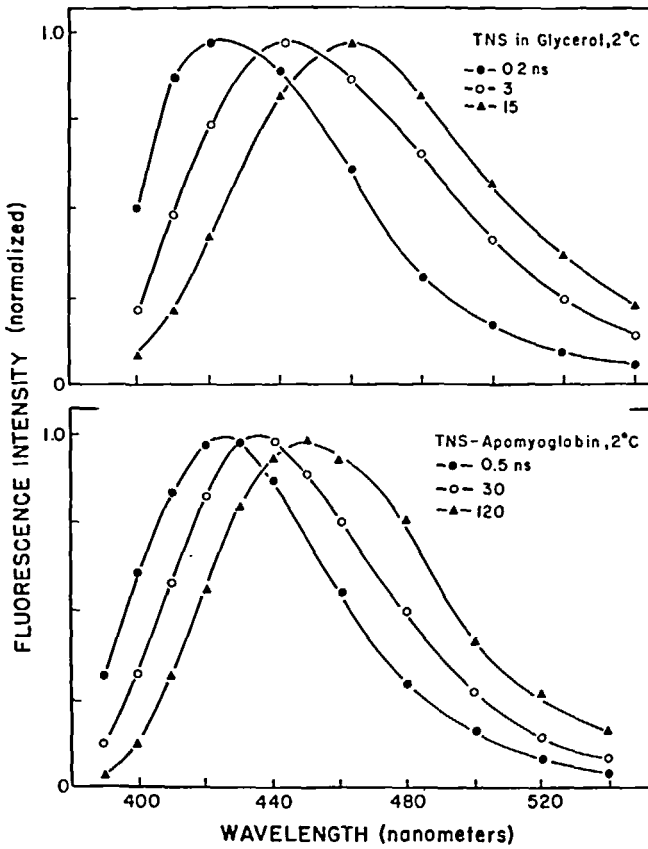functions (Figure 11). The frequency-domain data permitted

Figure 11

Time-Resolved Emission Spectra of TNS in Glycerol and TNS Bound to
Apomyoglobin.   From [27].

calculation of these spectra for times ranging from 0.1 nsec to
several times the average lifetime.   The emission spectra of TNS
in glycerol appear to relax more rapidly than that of TNS-labeled
apomyoglobin.   This difference is evident from the emission
spectra shown at 3 nsec for TNS in glycerol and at 30 nsec for
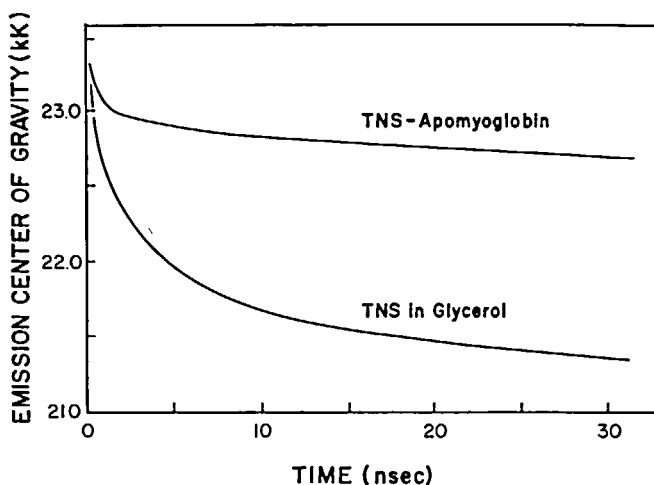TNS-apomyoglobin.   The spectra shift is about 50% complete at 3

Figure 12

Time-Resolved Emission Center-of-Gravity of TNS in Glycerol and
Bound to Apomyoglobin. From [27].

and 30 nsec for these different samples. The spectral decay is
more easily visualized by examining the time-dependent center-of-
gravity, $\bar{\nu}(t)$.This parameter is proportional to the average energy
of the emission. The decay of $\bar{\nu}(t)$ is more rapid in glycerol
than for TNS bound to apomyoglobin (Figure 12). A greater total
decay (in kK) is seen for TNS in glycerol than for TNS bound to
apomyoglobin.   Additionally,   the   center-of-gravity   of   TNS-
apomyoglobin shows an initially more rapid decay, followed by a
slower process which continues for at least 45 nsec. It is
difficult to precisely determine $\bar{\nu}(t)$ at these longer times, so
the observation of this slower process in apomyoglobin must be
regarded as preliminary. These results are in qualitative and
quantitive agreement with time-resolved measurements on similar
samples [48].

IV. CONCLUSION

Frequency-domain fluorometry provides impressive resolution of complex fluorescence decay kinetics, and is thus widely useful in chemical and biochemical research. The instrumentation is easily constructed from commercially-available components.

V. ACKNOWLEDGEMENTS

REFERENCES

1.   R.B. Cundall and R.E. Dale, Eds., "Time-Resolved Fluorescence Spectroscopy in Biochemistry and Biology", Plenum Press, N.Y., 1983.

2.   J.R. Lakowicz, "Principles of Fluorescence Spectroscopy, Plenum Press, N.Y., 1983.

3.   J.N. Demas, "Excited State Lifetime Measurements", Academic Press, N.Y., 1983.

4.   M.G. Badea and L. Brand, Methods Enzymol. 61, 378, 1979.

5.   R.R. Alfano, "Biological Events Probed by Ultrafast Laser Spectroscopy", Academic Press, New York, 1982.

6.   L.T. Libertini and E. Small, Rev. Sci. Instrum. 54, 1458, 1983.

7.   E.W. Small, L.J. Libertini and I. Isenberg, Rev. Sci. Instrum. 55, 879, 1984.

8.   A.v. Hoek, J. Vervoort and A.J.W.G. Visser, J. Biochem. Biophys. Methods 7, 243, 1983.

9.   A.J.W.G. Visser and A.v. Hoek, Photochem. Photobiol. 33, 35 1981.

10.   E.Z. Gaviola, Z. Phys. 42, 852, 1927.

11. E.A. Bailey and G.K. Rollefson, J. Chem. Phys. 21, 1315
     1953.

12. J.B. Birks and D.J. Dyson, J. Sci. Instrum. 38, 282, 1961.

13. A. Müller, R. Lumry and H. Kokubun, Rev. Sci. Instrum. 36,
     1214, 1965.

14. R.D. Spencer and G. Weber, Ann. N.Y. Acad. Sci. 158, 361,
     1969.

15. D.M. Jameson and E. Gratton, "Analysis of Heterogeneous
     Emissions by Multifrequency Phase and Modulation Fluoro-
     metery" In: New Directions in Molecular Luminescence, D.
     Eastwood, Ed. ASTP, Philadelphia, pp. 67-81, 1983.

16. D.M. Jameson and G. Weber, J., Phys. CHem. 85, 953, 1981.

17. J.R. Lakowicz and H. Cherek, J. Biol. Chem. 256, 6348, 1981.

18. J.R. Lakowicz, F.G. Prendergast and D. Hogen, Biochemistry,
     18, 508, 1979.

19. J.R. Lakowicz and H. Cherek, J. Biochem. Biophys. Methods,
     5, 19-35, 1981.

20. S. Keating-Nakamoto and J.R. Lakowicz, Analytical Bio-
     chemistry, in press, 1985.

21. E. Gratton and M. Limkeman, Biophys. J. 44, 315, 1983.

22. J.R. Lakowicz and B.P. Maliwal, Biophysical Chemistry, 21,
     61, 1985.

23. U.A.W. Klein, The Arabian Journal of Science and
     Engineering, 9, 327, 1984.

24. E.R. Menzel and Z.D. Popovic, Rev. Sci. Instrum. 49, 34,
     1978.

25. H.P. Haar and M. Hauser, Rev. Sci. Instrum. 49, 632, 1978.

26. E. Gratton, J.R. Lakowicz, B. Maliwal, H. Cherek, G. Laczko
     and M. Limkeman, Biophys. J. 46, 479, 1984.

27. J.R. Lakowicz, H. Cherek, B. Maliwal and E. Gratton,
     Biochemistry, 24, 376, 1985.

28. J.R. Lakowicz, H. Cherek, B.P. Maliwal, G. Laczko and E.
     Gratton, J. Biol. Chem. 259, 10967, 1984.

29. J.R. Lakowicz, H. Cherek, G. Laczko and E. Gratton, Biochim.
     Biophys. Acta 777, 183 1984.

30. P.R. Bevington, "Data Reduction and Error Analysis for the Physical Sciences", McGraw-Hill, New York, 1969.

31. S. Brant, "Statistical and Computational Methods in Data Analysis", North Holland, 1970.

32. J.R. Lakowicz, E. Gratton, G. Laczko, H. Cherek and M. Limkeman, Biophys. J. 46, 463, 1984.

33. J.R. Lakowicz and H. Cherek, J. Biochem. Biophys. Methods 5, 131, 1981.

34. I.P. Kaminov, "An Introduction to Electrooptic Devices", Academic Press, New York, 1974.

35. J. Wilson and J.F.B. Hawkes, "Optoelectronics, An Introduction", Prentice/Hall International, Englewood Cliffs, NJ, 1983.

36. G. Weber, J. Chem. Phys. 66, 4081, 1977.

37. V.V. Solodovnikov, "Introduction to the Statistical Dynamics of Automatic Control Systems", Dover Publication, New York, 1960.

38. J.H. Easter, R.P. DeToma and L. Brand, Biophys. J. 16, 571-583, 1976.

39. M.G. Badea and L. Brand, Methods in Enzymology, 61, 378, 1979.

40. J.R. Knutson, J.M. Beechem and L. Brand, Chem. Phys. Lett. 102, 501, 1983.

41. A. Grinvald and I.Z. Steinberg, Analytical Biochemistry 54, 583, 1974.

42. M.D. Barkley, A. Kowalczyk and L. Brand, J. Chem. Phys. 75, 3581, 1981.

43. J.R. Lakowicz and J.R. Knutson, Biochemistry 19, 905, 1980.

44. W.R. Ware, S.K. Lee, C.J. Brant and P. Chow, J. Chem. Phys. 54, 4729, 1970.

45. M.G. Badea, R.P. DeToma and L. Brand, Biophys. J. 24, 197, 1978.

46. J.R. Lakowicz and A. Balter, Biophysical Chemistry, 16, 99, 1982.

47.   J.R. Laws, and L. Brand, J. Phys. Chem. 83, 795, 1979.

48.   A. Gafni, R.P. DeToma, R.E. Manrow and L. Brand, Biophys. J.
      17, 155, 1977.